Computational Materials Science 46 (2009) 821–827

Contents lists available at ScienceDirect

Computational Materials Science

journal homepage: www.elsevier.com/locate/commatsci

Analyzing Fe–Zn system using molecular dynamics, evolutionary neural nets and multi-objective genetic algorithms

Baidurya Bhattacharya [a], G.R. Dinesh Kumar [b], Akash Agarwal [b], Şakir Erkoç [c], Arunima Singh [b], Nirupam Chakraborti [b,*]

[a] Department of Civil Engineering, Indian Institute of Technology, Kharagpur 721 302, India
[b] Department of Metallurgical and Materials Engineering, Indian Institute of Technology, Kharagpur 721 302, India
[c] Department of Physics, Middle East Technical University, 06531 Ankara, Turkey

ARTICLE INFO

Article history:
Received 24 February 2009
Received in revised form 6 April 2009
Accepted 15 April 2009
Available online 15 May 2009

PACS:
61.43.Dq
02.70.Ns
02.60.Pn
07.05.Mh

Keywords:
Fe–Zn system
Hot-dip galvanizing
Molecular dynamics
Multi-objective optimization
Artificial neural networks
Genetic algorithms

ABSTRACT

Failure behavior of Zn coated Fe is simulated through molecular dynamics (MD) and the energy absorbed at the onset of failure along with the corresponding strain of the Zn lattice are computed for different levels of applied shear rate, temperature and thickness. Data-driven models are constructed by feeding the MD results to an evolutionary neural network. The outputs of these neural networks are utilized to carry out a multi-objective optimization through genetic algorithms, where the best possible tradeoffs between two conflicting requirements, minimum deformation and maximum energy absorption at the onset of failure, are determined by constructing a Pareto frontier.

1. Introduction

Zinc forms a protective coating over steel. The technology of hot-dip galvanizing offering such protections is quite ubiquitous in the steel industries worldwide and adequately documented [1–3]. Although the phase relationships in Fe–Zn system are well known and the corresponding Phase diagram is readily available [4], it is still not exactly clear from a mechanistic approach, how far and how exactly such coatings would resist failure due to shear forces, in the form of wear, abrasion, fretting, etc., that routinely act on such coated structures. This study aims at bridging that gap by looking at the shearing process at the atomic level through molecular dynamics (MD) simulations. The idea is to design a coating that would absorb a large amount of shearing energy while exhibiting a small amount of shear deformation. A genetic algorithms [5–9] based bi-objective optimization strategy was utilized to tackle this problem, for which the objective functions were constructed through an evolutionary neural network [10–12].

2. Background

Simulating materials behavior through molecular dynamics has emerged as a powerful research strategy and numerous interesting applications have been reported in the recent past [13–15]. Several crucial physical and mechanical properties, ranging from stability to fracture toughness, could be arrived at for a wide range of materials using this approach, rendering it particularly attractive for modeling complex materials systems. In addition, through an MD simulation one can actually look into the temporal behavior of a material deformation process, for which the present investigation could be treated as a paradigm case, and that requires reliable processing of a large amount of simulation data that are often of highly non-linear nature. It is always cumbersome and sometimes very difficult to process the temporal information from an MD simulation using an analytical model, and a data driven modeling approach makes perfect sense in such a scenario, for which the

* Corresponding author. Tel./fax: +91 3222 283286
E-mail address: nchakrab@iitkgp.ac.in (N. Chakraborti).

0927-0256/$ - see front matter © 2009 Elsevier B.V. All rights reserved.
doi:10.1016/j.commatsci.2009.04.023

artificial neural networks (ANN) [16] are noted for their efficacy. An evolutionary version of ANN proposed recently [10] has already been applied successfully to a number of studies of materials interest [10–12,17,18] and is also deemed appropriate in the present context. Furthermore, the conflicting aspirations of the present problem, mentioned briefly in the previous section, would lead to a search for the best possible tradeoffs between each of them. These problems are known as multi-objective optimization problems, which are now a days increasingly being solved using biologically inspired genetic algorithms (GA). The genetic algorithms, in turn, are steadily gaining ground for the problems in the materials domain, as evidenced by a number of review articles published in recent times [5–9] and are selected in this work to carry out the optimization task owing to their robust and flexible nature. In this backdrop this study is constituted by the synergy among three independent paradigms: MD, ANN and GA, an approach which so far has not been tried out to any significant extent in the materials discipline, despite its pertinence to the processes like hot-dip galvanizing, or the systems like Fe–Zn that constitute the present work. The nature of the optimization task and the details of the adopted methodology are elaborated below.

2.1. The bi-objective optimization problem

Here the idea is to come up with a galvanized coat that would withstand a high amount of shear while exhibiting as little deformation as possible even at the onset of breaking. To achieve this, we simultaneously optimized the following objectives obtained through MD simulations:

- Maximize the energy absorbed till onset of failure, measured with respect to the equilibrated state (E).
- Minimize the extent of shear strain at the onset of failure (e).

The solution strategy would require some further elaboration.

3. Methodology

The selection of appropriate inter atomic potentials are crucial to an accurate modeling of atomistic systems. The Fe–Fe and Zn–Zn potentials were taken from the literature [20], while the Fe–Zn potential was developed in the course of this study using limited Density Functional Theory (DFT) calculations. All the three potentials are presented below.

Zn–Zn interaction: in this study the Morse potential [20] was used to model the pairwise interactions between the Zn atoms. This is expressed as:

$$E = D_0\left[e^{-2\alpha(r-r_0)} - 2e^{-\alpha(r-r_0)}\right] \quad r < r_c \tag{1}$$

where E is the interaction energy between the two atoms (eV), r denotes the distance between the two atoms (Å), r_0 is the equilibrium distance between the two atoms (Å), r_C is the cutoff distance (4.5 Å), while α, and D_0 are constants with respective dimensions of reciprocal distance (Å^{-1}) and energy (eV). The parameters used for this potential are listed in Table 1.

Fe–Fe interaction: to model the interaction between the BCC iron atoms the potential function of Embedded-Atom Method of Finnis and Sinclair (EAM/FS) [19] has been used. The relevant potential is expressed as:

$$E_i = F_\alpha\left(\sum_{j\neq i}\rho_{\alpha\beta}(r_{ij})\right) + \frac{1}{2}\left(\sum_{j\neq i}\phi_{\alpha\beta}(r_{ij})\right) \tag{2}$$

where E_i is the total energy of an atom i, (eV), F denotes the embedding energy (eV), ρ is atomic electron density, ϕ is the pair potential interaction, while α, β indicate element types of atoms i and j.

This potential is built in the molecular dynamics software LAMMPS (Large Scale Atomic/Molecular Massively Parallel Simulator) [21] used in this study where the various parameters for Fe–Fe interaction are also provided.

Fe–Zn interaction: in the absence of a reliable potential that could be incorporated in LAMMPS, a custom made potential was constructed during this research following a strategy explained elsewhere [22]. The pair potential energy function is given as:

$$U(r) = \left(\frac{A_1}{r^{\lambda_1}}\right)e^{-\alpha_1 r^2} + \left(\frac{A_2}{r^{\lambda_2}}\right)e^{-\alpha_2 r^2} \tag{3}$$

where $U(r)$ is in eV, r is the distance between two atoms (Å). The parameters for this potential are provided in Table 2 and have been obtained by the following procedure: the total energy of FeZn diatom has been calculated at various interatomic distances by DFT [23] with B3LYP exchange–correlation functional [24–25] using CEP-121G basis set [26]. After this procedure interaction energy of the pair has been calculated from the relation $E_{\text{int}}(r) = E_{FeZn}(r) - E(Fe) - E(Zn)$, which is equivalent to the pair potential energy, namely $U(r) \equiv E_{\text{int}}(r)$. Actually $U(r)$ has been fitted to the data generated by $E_{\text{int}}(r)$ by applying a non-linear least square fit method, then a single set of parameters, given in Table 2, has been obtained.

Since this potential was found to be very weak compared to Fe–Fe and Zn–Zn systems, we modified the parameters A_1 and A_2 slightly to increase the potential well depth. The adjusted parameters are given in Table 3.

Once the potentials were implemented in the LAMMPS environment the system was made ready for the MD simulations. The details are as follows.

3.1. The molecular dynamics simulations

The idea behind the MD simulations was to generate the objective functions for the subsequent optimization study. To begin the process an assembly of a few layers of Zn atoms placed above a block of BCC iron was allowed to equilibrate first as an NVE ensemble. A shear force was introduced to the equilibrated assembly by setting the top Zn layer in motion with constant velocity while

Table 1
Parameters used for the Morse potential.

D_0 (eV)	α (Å^{-1})	r_0 (Å)
0.091552277	2.17861958	2.65552272

Table 3
The adjusted parameters for Fe–Zn potential.

A_1 (adjusted)	A_2 (adjusted)
80.8407924	−25.3747893

Table 2
The derived potential parameters for the Fe–Zn potential given in Eq. (3). In this parameter set energy is in eV and distance is in Å.

A_1	A_2	λ_1	λ_2	α_1	α_2
70.8407924	−22.374789	1.54122119	4.84043227	0.60454249	0.0301663477

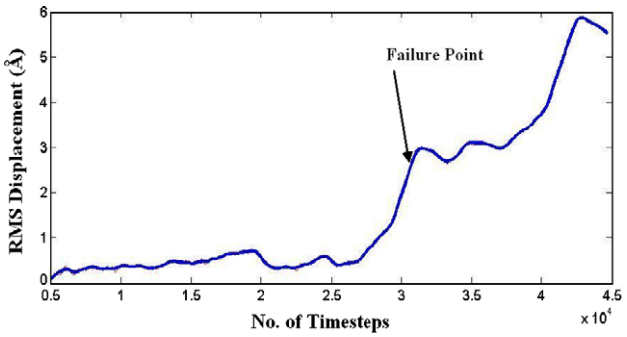

Fig. 1. A typical displacement profile for the interfacial layer of Zn after the onset of shear.

holding the bottom Fe layers fixed. The shearing continued by treating the system as an NPT ensemble and gradually propagated from layer to layer. No periodic boundary condition was employed. Initially the deformation of the Zn block was elastic in nature. As shearing continued, the relative displacement of the interfacial layer of Zn, just above iron reached the magnitude of the lattice parameter of Fe, and the Zn block slipped to a new position. This point may be taken as the onset of bond breaking and the point of shear failure. Since LAMMPS provides RMS displacement (δ_{rms}) for any specified group of atoms, the point of shear failure may be identified from the δ_{rms} vs. time plot for the interfacial Zn layer. A typical case is presented in Fig. 1. It should be noted at this point that raw data obtained from the MD simulation is often found to be noisy, rendering interpretation of the failure point rather ambiguous. This information therefore is smoothed using a local linear

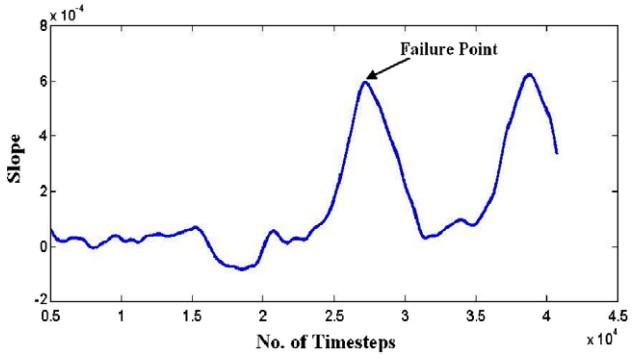

Fig. 2. The failure as a discrete event: the sharp peaks correspond to the points of failure.

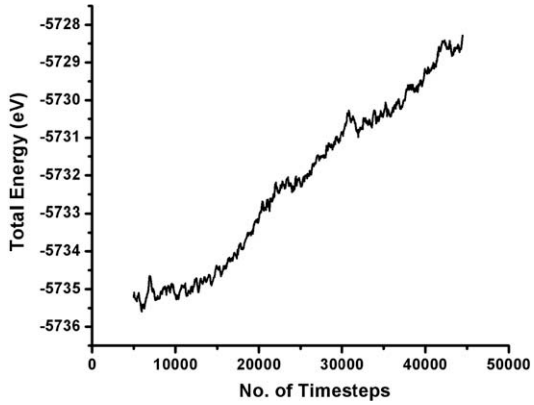

Fig. 3. Energy absorbed corresponding to Fig. 1.

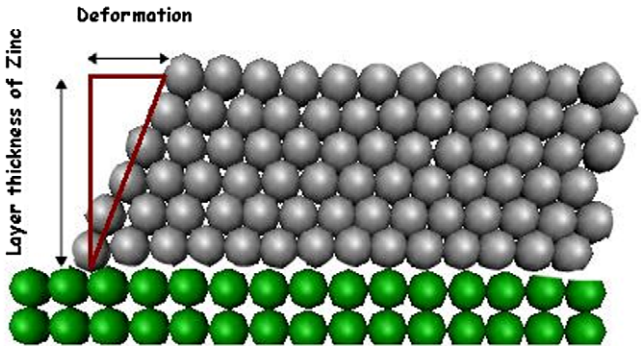

Fig. 4. Schematics of shear strain calculation.

Table 4
Molecular dynamics parameters.

Parameter	Range/description
Temperature	1–300 K
Lattice parameter of Fe (BCC)	2.860 Å
Lattice parameter of Zn (HCP)	2.621 Å
Atomic mass of Fe	55.845
Atomic mass of Zn	65.409
Boundary conditions	Periodic in all directions
Fe box dimension (in Å)	44*24*15
Zn box dimension (in Å)	33*x*11 (x varies from 7.4 to 21.4)
Time step	0.001 pico seconds
Time steps for equilibration	5000
Ensemble for equilibration	NVE
Ensemble for shear	NVT
Velocity for the top Zn layer (m/s)	1–100

least square regression routine (LOESS) available in the Curve Fitting Toolbox™ of MATLAB™ to come up with the plot shown in Fig. 1. The initiation of failure was taken as the instance when the displacement of the upper layer of atoms becomes equivalent to the lattice parameter. In most cases, the slope of the displacement plot sharply increases at the failure point, as shown in Fig. 2.

The energy of the system at that point provides the shear energy absorbed up to the point of failure, and gives the value of the first objective function in this study. A typical time history of total energy of system (E_T) corresponding to Figs. 1 and 2 is shown in Fig. 3 and as stated before, the energy needed for the failure (E) was taken as the difference between the energy at the failure point and that at the end of initial equilibration (i.e., at the onset of the shearing process).

If loading continues, failure occurs in discrete steps and the second peak in this figure corresponds to the next event.

Our second objective, the shear strain at failure (e) was computed as the ratio of deformation over Zn layer thickness, as explained schematically in Fig. 4.

The various parameters used in the MD simulations are provided in Table 4.

A large number of observations are actually needed to capture the extensive non-linearity in the objective functions. A total of 448 simulations were conducted during this study by changing the three variables: temperature, layer thickness and shear rate and the results were fed to an evolutionary neural net [10] and were subsequently optimized through a Predator-prey genetic algorithm [27], as detailed below.

3.2. Data capture through an evolutionary neural network

This approach differs significantly from the traditional neural nets [16]. As used in our earlier work [10–12], the architecture of

the neural network remains flexible and the training of the networks is undertaken following the principles of multi-objective genetic algorithms. To begin the process, one needs to initiate a population of neural networks, with a variable number of weights in their lower parts, which are subjected to some tailor-made crossover and mutation operations [28] and a fixed upper part where the training is done following linear least square algorithm [29]. The idea is to come up with a tradeoff between two conflicting requirements: a network with a maximum accuracy and minimum number of weights in its lower part. The choice in this case need not be unique. Formulated this way, the neural network training problem becomes a Pareto-optimal problem [30], where instead of a unique network, a family of networks, known as the Pareto-frontier, would represent the optimal solutions [30]. The members of the Pareto-frontier will be non-dominating [30] to each other and will not be dominated [30] by any other feasible solutions, which implies that none of the feasible solutions would offer any better compromise between the objectives than the Pareto-optimal solutions. Amongst themselves, any member of the Pareto-frontier can not be strictly better than another, even in terms of one objective, if it has to remain at least as good as the other member in terms of the remaining objectives. The mathematical formulation of Pareto-optimality is well known [30]. The way it is presented here utilizes the notion of weak dominance, which for a minimization problem is expressed as:

$$(\Omega_l \prec \Omega_m) \Longleftrightarrow (\forall_i)(f_{il} \leqslant f_{im}) \wedge (\exists_i)(f_{il} < f_{im}) \quad (4)$$

Here the objective functions are denoted by the f terms, and the vectors formed by the objectives comprise the Ω terms. If two solution vectors do not satisfy this relationship, they are considered non-dominating to each other. A family of solutions whose individual members are non-dominating to each other and at the same time not dominated by any other member in the feasible solution space, is taken as the Pareto set, and the locus of these individuals in the functional space constitutes the Pareto-frontier. Alternately one can construct the Pareto-optimality using the concept of strong dominance, requiring betterment or domination in terms of every objective. The weak formulation is however commonly used. More details are available elsewhere [30–31].

In the present case the Pareto-frontier for the training process was computed using a multi-objective Predator-prey genetic algorithm [10,27]. A similar algorithm was used later for optimizing the energy and strain at the point of failure, and will be discussed in due course. The trained neural nets are shown in Figs. 5 and 6. Each point in the frontiers presented in those figures denotes a neural net of distinct weights and architecture, providing the optimum tradeoff between the training accuracy and network size. Picking up one from the multiple options remains the job of the decision maker. In this study, like our earlier work [32] a suitable

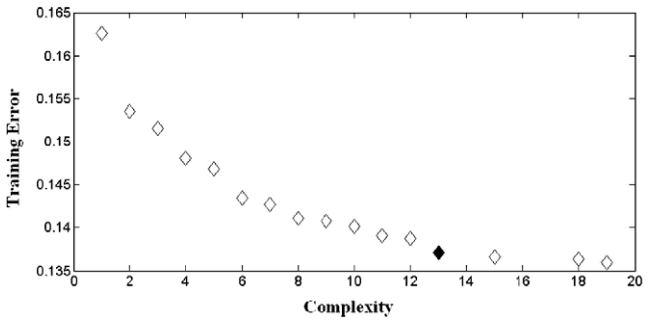

Fig. 5. Training of the objective function for energy using a bi-objective evolutionary neural network. The filled diamond denotes the network selected on the basis of information criteria.

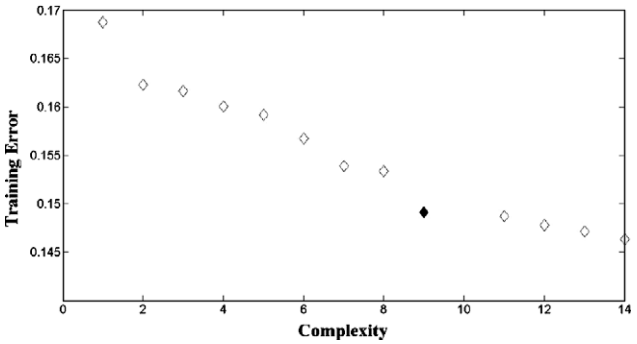

Fig. 6. Training of the objective function for strain using a bi-objective evolutionary neural network. The filled diamond denotes the network selected on the basis of information criteria.

network was identified using the Akaike's information criterion (*AIC*), the corrected Akaike's information criterion (*AICc*) and also the Bayesian information criterion (*BIC*) [33–35]. The basic strategy is outlined below.

3.3. The information criterion and the network of right complexity

A neural network could be both over and under parameterized, leading to unreliable predictions in both the situations. In case of noisy, non-linear data an over parameterized neural net would begin to capture the system noise, which is undesirable, while an un-

Table 5
Complexity analysis of the networks presented in Fig. 5. The selected network is boldfaced.

Complexity	*K*	*AIC*	*AICc*	*BIC*
1	13	1157.238	1158.191	1164.582
2	15	1121.824	1123.087	1132.445
3	16	1112.92	1114.356	1125.282
4	18	1106.495	1108.309	1122.521
5	20	1090.759	1092.999	1110.674
6	22	1094.914	1097.627	1118.917
7	23	1071.895	1074.863	1098.012
8	25	1077.874	1081.388	1108.346
9	27	1074.53	1078.638	1109.517
10	29	1075.869	1080.623	1115.521
11	30	1072.318	1077.414	1114.354
12	31	1063.177	1068.627	1107.63
13	**32**	**1062.396**	**1068.214**	**1109.299**
15	36	1066.147	1073.567	1123.153
18	38	1077.628	1085.931	1139.856
19	40	1062.782	1072.022	1130.337

Table 6
Complexity analysis of the networks presented in Fig. 6. The selected network is boldfaced.

Complexity	*K*	*AIC*	*AICc*	*BIC*
1	13	−946.133	−945.18	−938.788
2	15	−973.106	−971.843	−962.486
3	17	−972.112	−970.493	−957.947
4	19	−975.941	−973.919	−957.996
5	21	−976.35	−973.879	−954.415
6	22	−986.464	−983.751	−962.461
7	24	−997.067	−993.833	−968.794
8	26	−995.702	−991.897	−962.992
9	**26**	**−1017.98**	**−1014.18**	**−985.272**
11	30	−1012.16	−1007.06	−970.124
12	31	−1015.23	−1009.78	−970.775
13	33	−1014.76	−1008.57	−965.38
14	35	−1014.98	−1007.98	−960.546

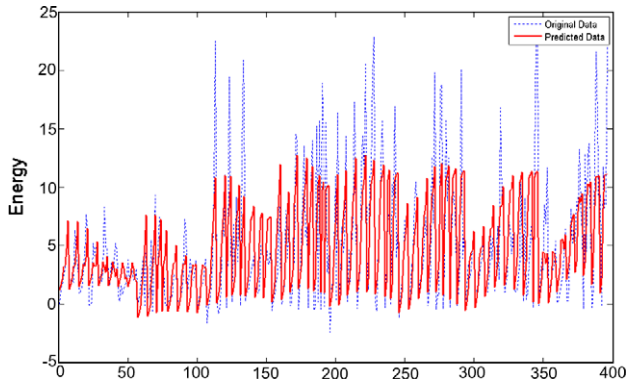

Fig. 7. Performance of the selected network for the energy data. The observation numbers are shown along the abscissa following real time data.

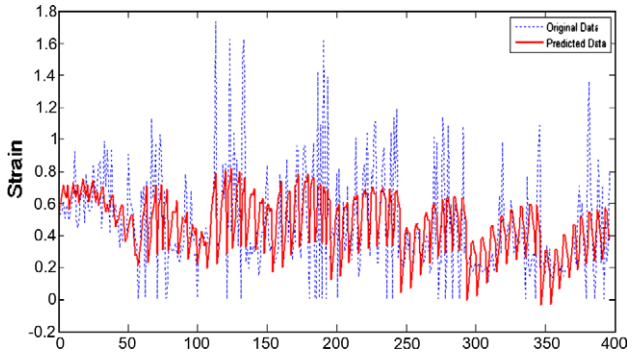

Fig. 8. Performance of the selected network for the strain data. The observation numbers are shown along the abscissa following real time data.

der parameterized network might not suffer from this problem, but would simply fail to capture its subtle nonlinearities. In this situation one can, in principle, be assisted by various information criteria that would allow the user to seek out for a network of right complexity. The three of them used in this study are expressed as:

$$AIC = 2k + n\ln\left(\frac{RSS}{n}\right) \tag{5}$$

$$BIC = k\ln k + n\ln\left(\frac{RSS}{n}\right) \tag{6}$$

$$AICc = AIC + \frac{2k(k+1)}{n-k-1} \tag{7}$$

where k is the number of parameters used in the network, taken as the total number of connections in both upper and lower parts of it, including the biases. n is the total number of observations and RSS is the residual sum of squares for the model.

The BIC criterion penalizes k more strongly than AIC and as a result, the AIC criterion often tends to produce a relatively over-parameterized model. This apparent weakness is remedied in $AICc$ by introducing a correction term in the AIC value, as shown in Eq. (7).

The information criteria of various networks along the Pareto-frontiers of Figs. 5 and 6 are summarized in Tables 5 and 6. As done on other occasions [10–12,17–18,32], here the complexity is expressed in terms of the number of connections in the lower part of the network, excluding the biases. The evolutionary neural network used in training [10] utilizes a fixed architecture in the upper part of the network and therefore could be excluded in the complexity assessment. A network of complexity 13 is adequate to represent the energy data, as suggested by all the three information criteria. In case of strain, the required complexity turns out to be eight. The chosen networks are specially marked in Figs. 5 and 6 and also in Tables 5 and 6. The performances of these two networks are further elaborated in Figs. 7 and 8 against the actual data.

3.4. Bi-criteria optimization of energy and strain through a Predator-prey genetic algorithm

Once the networks of right complexity were identified the next task was to optimize the objectives computed through them. This was done using a Predator-prey genetic algorithm [27], already tried out for a wide variety of problems [10–12,17–18], and as mentioned before, in this study, we have also used it for training the networks. This algorithm emulates the hunting behavior of

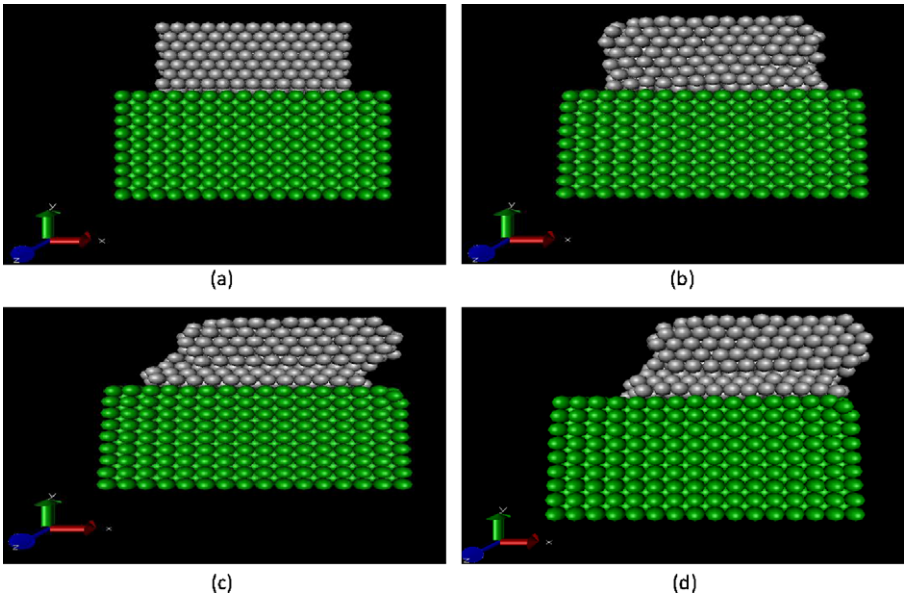

Fig. 9. The stages of shear failure. (a) Initial system with Zn above Fe (b) equilibrated system (c) continuation of shear process (d) after failure. The initial velocities are generated using random seed values at the specified temperature. The simulation box size (90*90*40 Å^3) is comparatively bigger than the lattices size of Fe and Zn.

the real-life predators and the natural responses of their prey, to compute the Pareto-frontier between two conflicting objectives which are E and e for the present problem. Both the predators and the prey reside in a two dimensional computational grid devoid of any physical meaning, where the prey denote the population of some probable solutions, and the predators, being some indestructible entities, are only out there to kill the weaker prey, where the weakness gets determined by the objective function values. A Moore neighborhood [36] is constructed for both the species, where they are allowed to move around following certain rules and the hunting takes place complying with some definite norms. The surviving prey population, after a round of killing, is allowed to breed, a privilege that is denied to the predators. The traditional genetic algorithms operators like crossover and mutation [5–9] are employed in the breeding stage and this cycle continues till an invincible prey population emerges withstanding generations of predator attack. The population is then ranked following any of the procedures described in the genetic algorithms literature [31] and the Pareto-frontier is formed by the best ranked members of this surviving population. Further details are available elsewhere [10].

4. Results and discussion

From the top of the equilibrated Zn layer where the shearing force was initiated by setting it into motion, the deformation proceeded downward and the process could be clearly visualized, as presented in Fig. 9 for a typical case. Although a number of binary phases are known to form in the Fe–Zn system [4], they remained rather inconsequential in the present simulations, since neither the length, nor the time scales studied here were conducive for any significant amount of diffusion to occur. The shearing effects however propagated from layer to layer, starting at the top and at the onset of failure the last zinc layer is set to motion. The presence of dislocations also has not been accounted for considering the length and time scales adopted here. Nonetheless, the adopted strategy is generic in nature and extendable to larger systems with more number of design variables, if adequate computing resources are available.

The computed Pareto-frontier between energy and strain are presented in Fig. 10. Both parameters are computed at the onset of failure, in a manner described in the previous section. The variable values along the Pareto frontier are presented in Table 7.

Along the Pareto frontier, as evident both from Fig. 10 and Table 7, an increase in energy required to failure comes at the expense of an increasing deformation. Point A which is near the origin of the frontier fails at a low value of energy and the corresponding deformation is also is also small. This however happens at a very small value of the Zn layer thickness (5.6505 Å) with a relatively small initial shear rate of 85.2532 m/s. With increasing thickness of the Zn layer, as evident from the typical points like B and C in Table 7, both the energy required for failure and the corresponding strain go up. The responses to these objective functions however are not monotonic with respect to the layer thickness. In fact, both energy and strain display a complicated interplay between all the three system variables, velocity, layer thickness and temperature with which the two objective functions, involving energy and strain, are correlated in a highly non-linear fashion. The evolutionary neural network [10] that we have used here enabled us to capture this implicit non-linearity more effectively than some of our recent material design work [37–39] and the efficacy of genetic algorithms as an optimizer, in such complex scenario is rather overwhelming, which is well in accord with the experiences of numerous researchers worldwide [5–9].

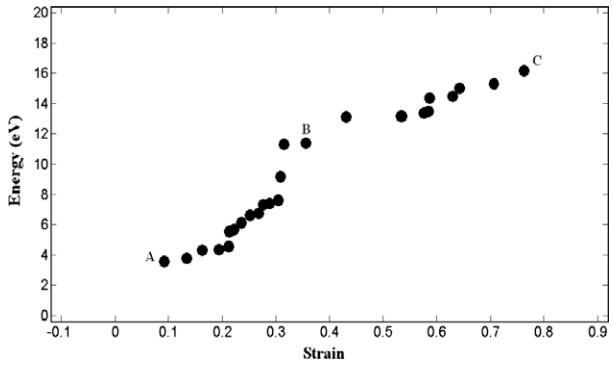

Fig. 10. The computed Pareto-frontier between energy and strain at the onset of failure.

Table 7
Variable values along the Pareto frontier shown in Fig. 10.

Position in Fig. 10	Velocity (m/s)	Temperature (K)	Layer thickness (Å)	Energy (eV)	Strain
A	85.2532	210.4119	5.6505	3.5853	0.0926
	112.7588	239.3733	9.5867	3.7669	0.1344
	67.7604	210.6762	4.3073	4.3189	0.1629
	106.3463	224.6426	9.8628	4.3459	0.194
	112.7588	224.7521	11.2589	4.5604	0.2122
	101.8124	243.7713	9.8793	5.5342	0.2134
	100.6397	242.3506	9.8705	5.6877	0.2217
	97.8143	247.3816	9.7075	6.1353	0.2359
	103.2256	239.7327	11.2589	6.6306	0.2521
	94.5417	241.3257	9.8628	6.7613	0.2677
	111.8975	229.4969	14.0304	7.3383	0.2761
	92.2102	247.4962	9.8628	7.4138	0.2877
	92.6062	235.7761	10.4598	7.6074	0.3039
	115.9127	221.291	17.3662	9.1844	0.3085
	105.8956	251.9936	20.4571	11.3306	0.3149
	96.0607	250.6466	15.1597	11.4208	0.3557
B	92.2102	255.7728	15.4982	12.2266	0.3814
	86.9755	294.5305	12.4989	13.119	0.4319
	72.8337	247.4962	14.9836	13.1779	0.5329
	72.5794	247.4962	14.9836	13.1912	0.5352
	68.1811	247.4962	14.9836	13.3906	0.5759
	67.1459	253.2253	15.9554	13.5198	0.584
	68.2145	267.3921	16.0829	14.3786	0.5871
	65.107	261.6798	12.2165	14.4964	0.6294
	64.3511	271.0959	15.0553	15.0409	0.6421
	60.4723	271.77	12.3234	15.327	0.7061
C	60.4723	294.5305	12.4989	16.1931	0.7628

Various Fe–Zn phases occurring in the binary phase diagram [4] are known to form in the galvanized sheets as well [40]. Although those are not considered in this study for reasons explained before, this analysis remains far from hypothetical. The η phase that is known to form at the top layer in the galvanized sheets is virtually pure Zn and the initiation of corrosion and the other environmental degradation processes [41] can locally bring it in contact with an iron rich phase, for which the findings of the present study would be quite relevant.

5. Concluding remarks

This study brings together two important soft computing paradigms, genetic algorithms and neural nets in the domain of classical molecular dynamics. Important physical and mechanical properties, ranging from stability to fracture toughness of complex materials systems, are now investigated through molecular dynamics for a wide range of materials [42,43]. The multi-objective approach used here offers far more flexibility than the more common single objective approaches used in materials design. This is increasingly being demonstrated by the materials researchers at large [6,8,44,45] and strategies like evolutionary neural network

as practiced here or response surface method adopted by the others [45] can further augment its scope. Despite enormous practical importance of the system studied here, the extent of relevant modeling work done on it is rather limited till now and that justifies the present attempt even from an industrial point of view. In the very near future we plan to substantially augment the model presented here by realistically bringing in the phase changes in the coated layer along with diffusion, which by any means, remains quite a complicated task.

Acknowledgement

Financial and logistic support from TATA Steel is thankfully acknowledged. One of the authors (SE) would like to thank TUBITAK (The Scientific and Technological Research Council of Turkey) for partial support through the project TUBITAK-TBAG-107T142.

References

[1] P. Bicao, W. Jianhua, S. Xuping, L. Zhi, Y. Fucheng, Surf. Coat. Technol. 202 (2008) 1785.
[2] H. Asgari, M.R. Toroghinejad, M.A. Golozar, Curr. Appl. Phys. 9 (2009) 59.
[3] E.M. Bellhouse, J.R. McDermid, Mater. Sci. Eng. A – Struct. 491 (2008) 39.
[4] G. Reumont, P. Perrot, J.M. Fiorani, J. Hertz, J. Phase Equilib. 21 (2000) 371.
[5] N. Chakraborti, Int. Mater. Rev. 49 (2004) 246.
[6] K. Mitra, Int. Mater. Rev. 53 (2008) 275.
[7] W. Paszkowicz, Mater. Manuf. Process. 24 (2009) 174.
[8] C.A. Coello Coello, R.L. Becerra, Mater. Manuf. Process. 24 (2009) 119.
[9] K.D.M. Harris, Mater. Manuf. Process. 24 (2009) 293.
[10] F. Pettersson, N. Chakraborti, H. Saxén, Appl. Soft Comput. 7 (2007) 387.
[11] F. Pettersson, N. Chakraborti, S.B. Singh, Steel Res. Int. 78 (2007) 890.
[12] M. Helle, F. Pettersson, N. Chakraborti, H. Saxén, Steel Res. Int. 77 (2006) 75.
[13] D.C. Rapaport, The Art of Molecular Dynamics Simulations, Cambridge University Press, Cambridge, 1995.
[14] Y. Mishin, Mater. Sci. Forum 502 (2005) 21.
[15] Ş. Erkoç, Mater. Sci. Forum 502 (2005) 51.
[16] J.A. Anderson, An Introduction to Neural Networks, Prentice-Hall, New Delhi, India, 2001.
[17] A. Agarwal, F. Pettersson, A. Singh, C.S. Kong, H. Saxén, K. Rajan, S. Iwata, N. Chakraborti, Mater. Manuf. Process. 24 (2009) 274.
[18] T. Stewart, O. Bandte, H. Braun, N. Chakraborti, M. Ehrgott, M. Góbelt, Y. Jin, H. Nakayama, S. Poles, D. Di Stefano, Lect. Notes Comput. Sci. (Including Subseries Lect. Notes Artif. Int. Lect. Notes Bioinformat.) LNCS 5252 (2008) 285.
[19] M.W. Finnis, J.E. Sinclair, Philos. Mag. A 50 (1984) 45–55.
[20] Ş. Erkoç, Annu. Rev. Comp. Phys. IX (2001) 1.
[21] http://lammps.sandia.gov.
[22] Ş. Erkoç, T. Bastug, M. Hirata, S. Tachimori, Chem. Phys. Lett. 314 (1999) 203.
[23] W. Kohn, L.J. Sham, Phys. Rev. 140 (1965) 1133.
[24] A.D. Becke, Phys. Rev. A 38 (1988) 3098.
[25] C. Lee, W. Yang, R.G. Parr, Phys. Rev. B 37 (1988) 785.
[26] W.J. Stevens, H. Basch, M. Krauss, J. Chem. Phys. 81 (1984) 6026.
[27] X. Li, Lect. Notes Comput. Sci. LNCS 2632 (2003) 207.
[28] S. Datta, F. Pettersson, S. Ganguly, H. Saxén, N. Chakraborti, Mater. Manuf. Process. 23 (2008) 130.
[29] F. Pettersson, H. Saxén, A hybrid algorithm for weight and connectivity optimization in feedforward neural networks, in: D.W. Pearson, N.C. Steele, R.F. Albrecht (Eds.), Artificial Neural Nets, Genetic Algorithms, Proceedings (International Conference on Artificial Neural Nets, Genetic Algorithms Roanne, France, April 23–25, 2003), Springer-Verlag, Vienna, Austria, 2003.
[30] K. Miettenen, Non-linear Multiobjective Optimization, Kluwer Academic Publishers, Boston, 1999.
[31] C.A. Coello Coello, D.A. Van Veldhuizen, G.B. Lamont, Evolutionary Algorithms for Solving Multi-objective Problems, Kluwer, New York, 2002.
[32] F. Pettersson, A. Biswas, P.K. Sen, H. Saxén, N. Chakraborti, Mater. Manuf. Process. 24 (2009) 320.
[33] H. Akaike, IEEE Trans. Autom. Control 19 (1974) 716.
[34] G. Schwarz, Ann. Statist. 6 (1978) 461.
[35] N. Sugiura, Commun. Statist. A – Theor. 7 (1978) 13.
[36] R. Dewri, N. Chakraborti, Model. Simul. Mater. Sci. 13 (2005) 173.
[37] N. Chakraborti, R. Sreevathsan, R. Jayakanth, B. Bhattacharya, Comput. Mater. Sci. 45 (2009) 1.
[38] R. Sreevathsan, B. Bhattacharya, N. Chakraborti, Mater. Manuf. Process. 24 (2009) 162.
[39] R. Sreevathsan, B. Bhattacharya, G. Dinesh Kumar, N. Chakraborti, J. Comput. Theor. Nanosci. 6 (2009) 849.
[40] F.H. Kao, W.C. Li, C.Y. Chen, C.Y. Huang, J.R. Yang, S.H. Wang, Mater. Sci. Eng. A 499 (2009) 45.
[41] U.K. Chatterjee, S.K. Bose, S.K. Roy, Environmental Degradation of Metals, Marcel Dekker, Inc., New York, 2001.
[42] Q. Lu, B. Bhattacharya, Eng. Fract. Mech. 72 (2005) 2037.
[43] Q. Lu, B. Bhattacharya, Nanotechnology 17 (2006) 1323.
[44] F. Pettersson, C. Suh, H. Saxén, K. Rajan, N. Chakraborti, Mater. Manuf. Process. 24 (2009) 2.
[45] G.S. Dulikravich, I.N. Egorov, M.J. Colaço, Model. Simul. Mater. Sci. 16 (2008) 12 (Article number 075010).